How to cite: *Angew. Chem. Int. Ed.* **2021**, *60*, 14938–14944
International Edition: doi.org/10.1002/anie.202012852
German Edition: doi.org/10.1002/ange.202012852

Analytical Methods

A Dual Fluorescence–Spin Label Probe for Visualization and Quantification of Target Molecules in Tissue by Multiplexed FLIM–EPR Spectroscopy

Pin Dong[+], Johannes Stellmacher[+], Lydia M. Bouchet[+], Marius Nieke, Amit Kumar, Ernesto R. Osorio-Blanco, Gregor Nagel, Silke B. Lohan, Christian Teutloff, Alexa Patzelt, Monika Schäfer-Korting, Marcelo Calderón, Martina C. Meinke,* and Ulrike Alexiev**

Abstract: *Simultaneous visualization and concentration quantification of molecules in biological tissue is an important though challenging goal. The advantages of fluorescence lifetime imaging microscopy (FLIM) for visualization, and electron paramagnetic resonance (EPR) spectroscopy for quantification are complementary. Their combination in a multiplexed approach promises a successful but ambitious strategy because of spin label-mediated fluorescence quenching. Here, we solved this problem and present the molecular design of a dual label (DL) compound comprising a highly fluorescent dye together with an EPR spin probe, which also renders the fluorescence lifetime to be concentration sensitive. The DL can easily be coupled to the biomolecule of choice, enabling in vivo and in vitro applications. This novel approach paves the way for elegant studies ranging from fundamental biological investigations to preclinical drug research, as shown in proof-of-principle penetration experiments in human skin ex vivo.*

Introduction

The quantification of molecules of interest in tissue usually requires invasive procedures, including time-consuming steps of tissue homogenization, and performing analysis such as chemical extraction of the sample. Current methods in preclinical research often lack a proof of translatability to human,[1] which contributes to the poor success rates in clinical studies. Method validation is thereby often neglected while found to be essential as the real concentration at the target site remains unknown.[1] Therefore, spectroscopic techniques for direct, non-invasive, and spatially resolved concentration quantification are highly desirable. While EPR allows to quantify the absolute number of spin-labeled molecules in tissue without homogenization and extraction, as shown for nanocarriers and drugs in skin,[2] it has a limited spatial resolution of approximately 50–100 μm.[3] The use of conventional fluorescence microscopy as a direct quantitative tool for concentration determination in tissue has been explored but remains challenging, except in certain cases,[4] mostly due to scattering and absorption of the excitation and the emitted fluorescence light, as well as the autofluorescence in the tissue.[5] However, fluorescence lifetime imaging microscopy (FLIM) has received a lot of attention in the recent years as a sensitive tool for visualizing the spatial distribution of endogenous and exogenous fluorescent molecules at the subcellular and suborganelle level.[6] This sensitivity and signal specificity of FLIM relies on the fluorescence lifetime as an intrinsic property of a given

[*] Dr. P. Dong,[+] Dr. S. B. Lohan, Dr. A. Patzelt, Prof. Dr. M. C. Meinke
Department of Dermatology, Venereology and Allergology, Charité Universitätsmedizin Berlin, corporate member of Freie Universität Berlin, Humboldt-Universität zu Berlin, and Berlin Institute of Health
Berlin (Germany)
E-mail: martina.meinke@charite.de

Dr. P. Dong,[+] Prof. Dr. M. Schäfer-Korting
Freie Universität Berlin, Institute of Pharmacy
Berlin (Germany)

J. Stellmacher,[+] M. Nieke, Dr. C. Teutloff, Prof. Dr. U. Alexiev
Freie Universität Berlin, Institute of Experimental Physics, Department of Physics
Berlin (Germany)
E-mail: ulrike.alexiev@fu-berlin.de

L. M. Bouchet,[+] A. Kumar, E. R. Osorio-Blanco, G. Nagel, Prof. Dr. M. Calderón
Freie Universität Berlin, Institute of Chemistry and Biochemistry
Berlin (Germany)

M. Nieke
Humboldt-Universität zu Berlin, Institute of Biology
Berlin (Germany)

Prof. Dr. M. Calderón
POLYMAT, Faculty of Chemistry, University of the Basque Country, UPV/EHU
20018 Donostia-San Sebastián (Spain)
and
IKERBASQUE, Basque Foundation for Science
48013 Bilbao (Spain)
E-mail: marcelo.calderon@polymat.eu

[+] These authors contributed equally to this work.

Supporting information and the ORCID identification number(s) for the author(s) of this article can be found under: https://doi.org/10.1002/anie.202012852.

fluorophore that is usually independent of fluorophore concentration and optical loss in the sample,[7] and inter alia provides discrimination between background fluorescence from molecules that naturally reside in tissue and the target fluorescence.[5d,8] Moreover, fluorescence lifetime is sensitive to the environment,[6b,c,9] as is EPR.[10] EPR provides information about the surrounding microenvironment of the spin-labeled molecule, such as polarity, pH, and viscosity, which can be inferred from the spectral shape, hyperfine coupling constant, g-tensor, and rotational correlation time of the EPR signal.[2,10,11] The changes in fluorescence lifetime offer insight into the microenvironment of the fluorophore, including pH, polarity, viscosity, biomolecular interactions, or reactive oxygen species.[6,9] However, this environmental sensitivity may also interfere with concentration determination in FLIM.

Up to now, the biomolecule of interest in general is singly labeled: a fluorophore label for studying biomolecular dynamics and interactions,[9a,d,12] or visualization and tissue distribution by FLIM;[6c,9c,13] and a spin label for quantification of target molecules in tissue or their dynamics by EPR.[2,10,11,14] However, individual labeling of the molecule of interest with a fluorophore or spin label could change its physicochemical properties, such as the log*P* (log octanol–water partition coefficient) value, and thereby tissue penetration.[15] Combining the strength of FLIM and EPR, we envisioned a dual label (DL) for multiplexed FLIM and EPR measurements (Figure 1) overcoming those risks.

Herein, we developed a general platform for synthesizing a dual label compound (DL), which realizes the simultaneous investigation by FLIM and EPR. We present the design, synthesis and photophysical properties of DL. The major challenge for a dual fluorescence–spin label is fluorescence deactivation by the unpaired electron of the spin label, a process which is usually employed in fluorescence quenching studies.[9e,16] We show that in contrast to other tested spin label–fluorescent dye combinations, such as fluorescein and 3-Carboxy-Proxyl (PCA), the combination of Rhodamine B (RhoB) and PCA (Figure 2) yields high fluorescence and spin probe stability. Very importantly, upon PCA conjugation

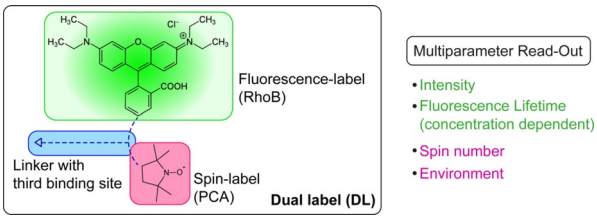

Figure 1. Fluorescence label (Rhodamine B, RhoB) properties, intensity and fluorescence lifetime, can be tuned to be both true concentration sensitive when in conjugation with a spin label (3-carboxy-proxyl, PCA). Colors mark the read-out parameters of each label. The resulting dual label (DL) probe provides non-destructive target detection and quantification as well as characterization of local environment in tissue via FLIM and EPR. Besides tissue applications, a DL-labeled biomolecule enables in vitro spectroscopic studies of the biomolecular conformation, structure, and dynamics.

RhoB is turned into a concentration dependent fluorescence lifetime probe.

The characterization of this RhoB containing DL is further accompanied by proof-of-principle experiments in skin tissue—a tissue that is highly relevant in topical drug application and the development of dermal and transdermal drug delivery systems.[2,13b,17] In the aged population, tissues including skin and mucous membranes of the oral cavity are prone to tumors,[9f,18] but 96% of anticancer drug candidates from preclinical studies fail in human.[19] DL labeling for insight into spatially resolved tissue concentrations quantified by EPR and FLIM offers an approach to method validation.[1] In particular, preclinical drug development will take significant profit from a larger spectrum of analytical methods with high spatial resolution and responding to concentration and environmental changes.

The experiments in tissue-mimicking agarose gel samples as well as in skin tissue revealed a highly consistent determination of DL concentration by both techniques, and the spatial distribution of DL in different tissue layers. Furthermore, the combination of EPR and FLIM in multi-

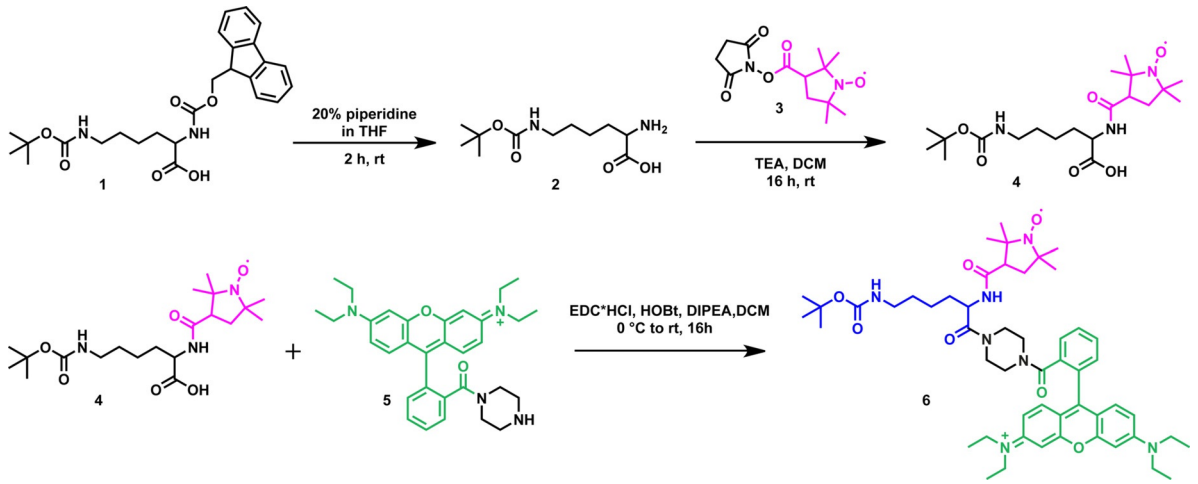

Figure 2. Scheme of DL synthesis. PCA (**3**) and Rhodamine B-piperazine (**5**) were covalently linked to Fmoc-Lys(Boc)-OH (**1**) yielding the DL conjugate (**6**). (**2**) deprotected Lys(Boc)-OH, (**4**) Boc-Lys-PCA.

plexed FLIM–EPR experiments enabled us to evaluate the microenvironments of the DL in the different tissue layers.

Thus, our novel platform for dual-labeled compounds will provide unprecedented insight into the tissue distribution of biomolecules, their concentration and microenvironment due to multiplexed FLIM and EPR spectroscopy, both in fundamental and applied research.

Results and Discussion

To develop a dual fluorescence-spin label compound for accurate concentration determination and simultaneous visualization of molecules in tissue (Figure 1), we first had to establish a platform for synthesizing the DL. We describe the synthesis and characterization of the tri-functional linker that contains the spin label PCA, a fluorescent molecule, and a third open labeling position for the conjugation to a biomolecule, drug or nanocarrier of choice. As shown in Figure 2, the synthesis can be split into two general processes: a) activation and conjugation of PCA and b) modification and conjugation of a fluorescent dye (the fully detailed synthesis conditions of each step can be found in the SI Experimental procedures). Both, the conjugation of PCA and the dye to lysine were conducted via a stable amide linkage. In the first step, after Fmoc deprotection of **1** according to literature (95% yield),[20] the NHS (N-hydroxysuccinimide)-activated PCA (**3**) was introduced via amide bond formation to give **4** as a yellow oil (81% yield). In the next step a fluorescent dye is covalently attached to **4**. In a first trial, 6-amino-fluorescein was attached through an amide bond to the carboxylic acid of compound **4**, expecting that the covalent attachment of 6-aminofluorescein yields a fluorescent conjugate.[21] Unfortunately, neither fluorescence increase upon attachment nor an active spin-probe were observed (Figure S1). This may be due to quenching effects on the reactions of the PCA radical by the aminofluorescein derivative. For a successful fluorescence labeling, we used a piperazine linker between the fluorophore and the spin probe. RhoB was functionalized with piperazine (**5**) to allow stable amide bond formation with the COOH group of lysine and to avoid pH-driven cyclization that forms a non-fluorescent adduct. The functionalization of **5** was performed using EDC (ethylene dichloride)-HCl, DIPEA (diisopropylethylamine), and HOBt (1-hydroxybenzotrazole hydrate), during 16 h reaction at room temperature. Furthermore, the fluorescent dye was covalently attached to **4**. The DL (**6**) was obtained as a purple solid (76% yield) after chromatographic purification. Importantly, the tert-butanol ester bond in the DL provides the third labeling position, after deprotection. All characteristic signals of DL were identified in the ^{1}H NMR and mass spectra (Figure S2–11). The log *P*-value (log octanol–water partition coefficient) of 0.07 ± 0.05 for DL reveals good water solubility. Furthermore, we demonstrated the stability of DL against endogenous tissue enzymes (Figure S12, Table S1).

In Figure 3, we present the spectroscopic characterization of the DL and its precursors in aqueous solution. The addition of the piperazine linker to RhoB at its carboxy-phenyl group (RhoB-pip, **5**) leads to a bathochromic shift compared to the

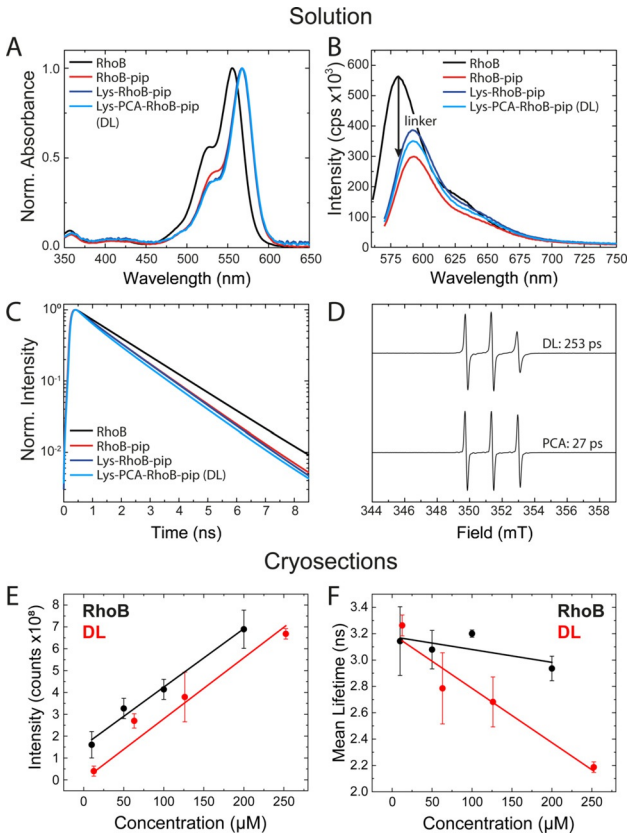

Figure 3. Characterization of DL in phosphate-buffered saline (PBS) solution and in cryosections from tissue mimetics (agarose gels). A) Normalized absorbance spectra of Rhodamine B (Rho B), DL (**6**), Rhodamine B-piperazine (**5**), and Boc-Lys-RhoB-piperazine for comparison. B) Emission spectra of the compounds shown in (A) at 10 or 12.6 μM (DL). C) Fluorescence decay curves of the compounds shown in (A). D) EPR spectra of 504 μM DL (**6**) and PCA dissolved in PBS. The correlation time is given. E) Concentration dependence of the fluorescence intensity of RhoB and DL from tissue mimetics using FLIM. F) Concentration dependence of the fluorescence lifetime of RhoB and DL in cryosections from tissue mimetics using FLIM. The errors bars are ± SD ($n = 3$).

RhoB spectrum, yielding an absorbance maximum at $\lambda_{abs} = (567 \pm 1)$ nm and an emission maximum at $\lambda_{em} = (592 \pm 1)$ nm (Figure 3A, B). A decrease of the fluorescence decay time from $\tau = 1.7$ ns for RhoB[22] to $\tau = 1.49$ ns for RhoB-pip (**5**) was observed (Figure 3C, Figure S13, Table S2) and consistent with known effects on RhoB emission, quantum yield, and fluorescence lifetime depending on the condition of the carboxy-phenyl group.[23] The addition of the Boc-Lys linker and PCA changed the absorption, emission, and fluorescence only slightly (Figure 3A–C, Table S2). DL exhibits a $\lambda_{abs} = (566 \pm 1)$ nm and $\lambda_{em} = (590 \pm 1)$ nm (Figure 3A, B), a fluorescence lifetime of $\tau = 1.41$ ns (Figure 3C, Table S2), and a quantum yield $\varphi = 0.18 \pm 0.03$ in water, which was determined using RhoB in ethanol[23a] as reference. The main reduction of RhoB fluorescence in aqueous solution stems from the conjugation to the piperazine linker (Figure 3B). Compared to the RhoB fluorescence, the DL fluorescence is reduced only by a factor of about two (Figure 3B), taking the respective extinction coefficients of RhoB and DL into

account (SI Experimental procedures). Thus, DL exhibits good fluorescence in phosphate buffered saline (PBS).

Figure 3D shows the EPR spectra of DL and PCA alone. The spectra exhibit the typical three peaks of the nitroxide spin, meaning that the chemical synthesis did not destroy the unpaired electron of PCA. A quantitative EPR analysis reveals about 60% of the spin labels being active after DL synthesis (SI Experimental Procedures, Figure S14, S15). Since stability tests of the spin label (Figure S16) show no further losses, the DL concentrations from EPR in Figure 4F–H were calculated by taking the 60% active spin label into account (see SI Experimental procedures). The high magnetic field peak of DL had a lower peak-to-peak height in comparison to the unlabeled PCA (Figure 3D). By simulating the EPR spectra of PCA and DL (see SI Experimental procedures), the rotational correlation time of DL was about ten times slower than for PCA free in solution, indicating that the mobility of PCA in the DL was reduced because of the neighboring covalently bound Fmoc or RhoB moiety. Taken together, the results shown in Figure 3 demonstrate the establishment of a novel platform to synthesize a functional dual fluorescence-spin label probe.

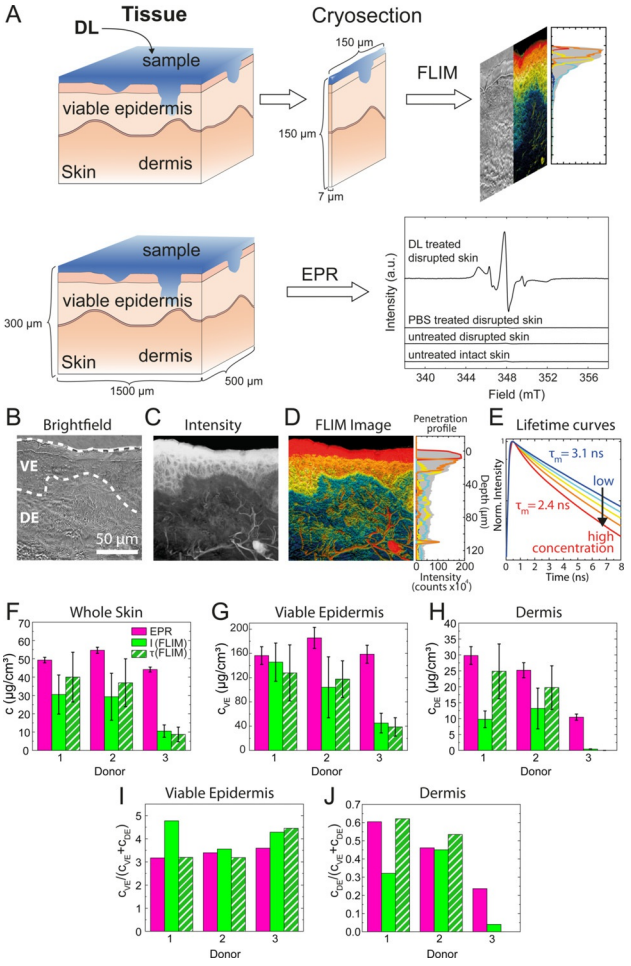

Figure 4. Localization and quantification of DL in human skin by EPR and FLIM. A) Sample preparation of skin after DL penetration, EPR measured whole tissue blocks, while for FLIM measurements cryosections were used. B) Brightfield, C) fluorescence intensity, and D) FLIM image with penetration profile. E) Fluorescence lifetime curves from the FLIM cluster image in (D). The concentration calibration is shown in Figure 3E,F and Figure S18. Comparison of DL concentration in F) whole skin, G) viable epidermis (VE), and H) dermis (DE), determined by EPR and fluorescence lifetime and intensity from FLIM. Error bars are ± SD ($n=4$). I,J) DL concentrations from (G) and (H) normalized to whole skin.

Next, we performed proof-of-principle experiments in human skin. The determination of DL concentration in skin via fluorescence requires the following two factors to be known: a) the stability of DL upon incubation with skin, and b) the correlation of fluorescence intensity and lifetime with DL concentration. We investigated the DL stability by comparing the absorbance and emission of the DL solution under conditions mimicking the skin penetration experiment (Figure S17). We found a decrease in fluorescence intensity over time upon the exposure of the DL solution to normal air, probably due to oxidation. Fluorescence intensity of the DL decreased by a factor of $F_r = 1.8$ after 2 h of incubation at 32 °C, while the fluorescence lifetime remained unchanged (Figure S17). To correlate the fluorescence read-out with concentration, we prepared varying concentrations of DL and RhoB from 10 to 253 µM in agarose gels, which simulate tissue samples (Figure S18). The fluorescence intensity increased linearly with concentration for RhoB and DL (Figure 3E). The fluorescence lifetime of RhoB was almost invariant to its concentration in the range up to 250 µM, in agreement with literature data for RhoB.[24] However, DL exhibited a shorter fluorescence lifetime with increasing DL concentrations in the same concentration range (Figure 3F and Figure S18). Thus, in addition to FLIM-based visualization, we can utilize the DL fluorescence intensity and lifetime as a concentration measure in tissue. DL concentration was calculated from the fluorescence intensity of the FLIM images according to Equation (1):

$$c_{DL}(I) = \frac{I_{ROI}/\ \#pixel\ in\ ROI \times image\ pixel}{\alpha} \times \mathrm{MW} \times F_r, \qquad (1)$$

where I_{ROI} is the fluorescence intensity in the region of interest (ROI), such as whole skin, viable epidermis or dermis, MW is the molecular weight, and α and b are slope and intercept of a linear fit of the concentration calibration data (Figure S18) with $b = 0$ for Equation (1). The FLIM lifetime data were analyzed by a cluster algorithm,[5d,8] which allows us to separate image pixel according to discrete lifetime clusters. We calculated the concentration from the lifetime data using Equation (2):

$$c_{DL}(\tau) = \sum_{cluster} \frac{\left(\frac{\tau_{cluster} - b}{\alpha}\right) \times \#pixel_{cluster}}{total\ \#pixel\ in\ ROI} \times MW \times F_r, \qquad (2)$$

where $\tau_{cluster}$ is the mean fluorescence lifetime of a given fluorescence cluster (see SI Experimental procedures) and $\#pixel_{cluster}$ are the corresponding number of pixels of this cluster, α and b are slope and intercept of a linear fit to the lifetime-based concentration calibration data (Figure S18).

For efficient DL penetration in skin, barrier disrupted human skin was used whose stratum corneum was removed

by cyanoacrylate glue (Figure S19–20). Figure 4A depicts the sample preparation for FLIM and EPR measurements. In EPR, whole tissue blocks were measured, while cryosections of the skin sample were used for FLIM measurements. The EPR spectrum of DL in skin represents a superposition of narrow and broad spectral lines, indicating that the DL resides in different microenvironments in the skin. Figure 4B–D visualizes DL skin penetration using FLIM, providing a spatially resolved image of DL distribution in the tissue (Figure 4D). Cluster-FLIM enhances the image contrast as well as statistical significance,[5d,8] thereby resolving detailed skin structures (Figure 4D). The highest DL concentration is depicted by the red fluorescence decay cluster in the false-color coded image with the fastest fluorescence decay time, while the lowest concentration is shown in blue with the slowest fluorescence decay time (Figure 4D, E). The concentration gradient from red to blue as determined from the calibration (Figure S18) follows the penetration profile, i.e., the highest concentration is found in the upper layers of the viable epidermis (VE), while low but significant concentrations are found in the dermis. As faster fluorescence lifetimes are also found in filament-like structures in the dermis (DE), presumably collagen and elastin fibers, we assume DL accumulation at these sites.

The absolute concentrations of DL in whole skin as well as in the viable epidermis and dermis (c_{VE} and $c_{DE,}$ respectively) were quantified by EPR and FLIM (Figure 4F–H). Both fluorescence-based methods are in good agreement with each other and for each donor in whole skin. We found the concentrations of DL in the skin based on EPR and fluorescence approaches to be consistent with each other within 2σ, except for donor #3. At lower DL concentrations within the dermis (Figure 4H), the fluorescence lifetime-based concentration determination is in very good agreement with EPR quantification. We also compared the relative distribution of the DL concentration in the different skin layers, i.e., viable epidermis and dermis, in a normalized plot of concentration (Figure 4I, J). Here, the data reveal a very good agreement between EPR and FLIM in the viable epidermis for all three donors (Figure 4I). We estimated that minimum concentrations in the lower µM to 100 nM range can be determined from EPR and FLIM using the DL.[9e,25]

The apparent heterogeneous inter-donor penetration behavior of donor #3 may be due to the fact that sample penetration heterogeneities would be more pronounced in cryosections, as used for FLIM, than in the integral concentration determination in EPR (Figure 4A). Another reason could be follicular penetration, which was so far unaccounted for in the cryosections. As shown in Figure 5A,B, the follicular and transfollicular penetration was significant (18-fold higher concentration compared to surrounding tissue) for the barrier disrupted skin used in this work. Compared to the FLIM measurements on cryosections, the EPR measurements on tissue blocks could involve DL accumulation within the hair follicles and its surroundings. However, even if considerably higher DL (Figure 5A, B) can be found in hair follicles, they only contribute to 1–14% of the skin surface depending on body site,[26] such that DL penetration would be increased by about 5%. Thus, everything considered, our quantitative results of DL skin penetration were consistent between EPR and FLIM.

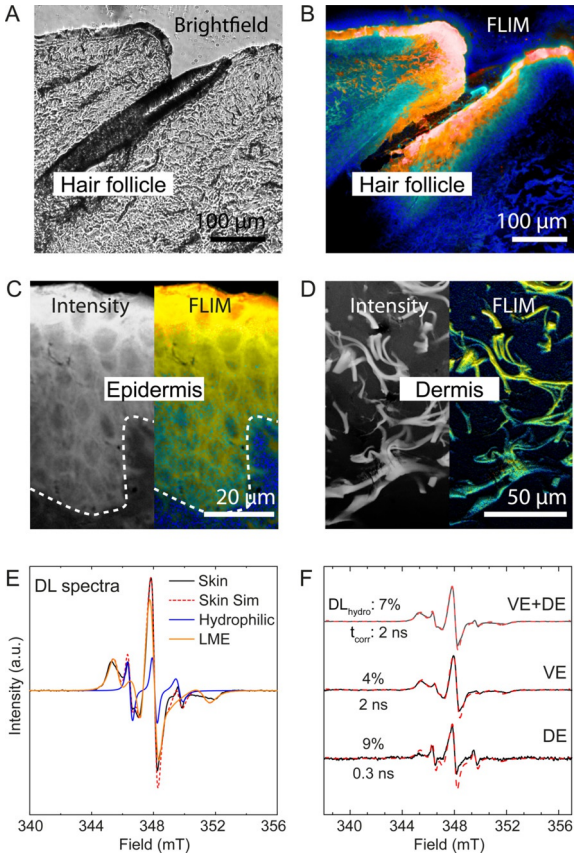

Figure 5. Sites of DL accumulation. A) Brightfield and B) FLIM images of a hair follicle of the same ROI. C) The viable epidermis and D) the dermis shown by FLIM. E) EPR spectrum of DL in whole skin is a linear combination of pure spectra of DL in a hydrophilic, fast mobility (DL_{Hydro}) or less polar, low mobility environment (LME). F) Experimental (solid lines) and simulated (dotted lines) EPR spectra of DL in the viable epidermis (VE) and dermis (DE). All spectra were normalized to the maximum peak intensity. The fraction of DL_{Hydro} and the corresponding rotational correlation time (t_{corr}) in different skin layers are indicated.

Besides spin label counting, EPR provides information about the microenvironment of the spin label. Combined with the high spatial resolution and contrast enhancement of FLIM, we were also able to obtain details about the environment of the DL at the subcellular level. Figure 5C shows the localization of the DL in the viable epidermis, both in the intercellular space and the cytoplasm of keratinocytes, which was verified in monolayer experiments (Figure S21). In the dermis, collagens and elastins exhibit a notably strong DL fluorescence signal, while DL was not identified in local skin cells, i.e., fibroblasts or macrophages (Figure 5D). By simulating the EPR spectrum (SI Experimental procedures, Table S3), DL was found to be surrounded by two different microenvironments (Figure 5E).

In the first microenvironment, DL had a hyperfine coupling constant (a_{zz}) of 100 MHz and a rotational correlation time (t_{corr}) (see SI Experimental procedures)[27] of 9 ns, representing DL with low mobility in a slightly apolar

environment, compatible to a restricted microenvironment with lipids, hydrophobic proteins, and less water content. In the other microenvironment, DL had an a_{zz} of 105 MHz and a smaller t_{corr} of 0.3–2 ns, indicating DL with high mobility in a hydrophilic microenvironment (DL_{Hydro}). The t_{corr} of DL_{Hydro} in the DE was shorter (0.3 ns) than in the VE ($t_{corr} = 2$ ns), indicating a higher water content and thus enabling a higher mobility. DL_{Hydro} was found with (4 ± 3)% in the viable epidermis, and this fraction increased in the dermis (Figure 5F, Table S3). The less hydrophilic environment in the viable epidermis is well in line with previous data.[28] Thus, the environmental sensitivity of the spin label was compatible with the main distribution of DL in the viable epidermis and within dermal collagen, as shown by FLIM (Figure 5C, D).

Conclusion

This work realizes the functional chemical synthesis of both a fluorophore and a spin marker into one compound, that we call dual label. This strategy provides the possibility of multiplexing FLIM and EPR in tissue investigations, for example, in skin penetration experiments for drug delivery. The amount of DL penetrating into different skin layers quantified by FLIM was in very good agreement with EPR. The spatial distribution of DL based on FLIM and its visualized accumulation sites yields a holistic image of the DL diffusion and interaction pattern when combined with EPR spectra simulations of DLs microenvironment. This is, for instance, of utmost importance when investigating anticancer drugs in preclinical studies. 3D tissue models, for example, tumor models to replace animal models, are getting more important. Here, the dual label could be a valuable tool to understand drug and carrier distribution which could give information with respect to treatment efficiency and development of treatment resistance; in particular, for macromolecular drugs for which the penetration into tissue is critical. In-depth insight into drug diffusivities and physical parameters determining drug distribution in tissue[28] could be obtained in the future from DL concentration data. Besides the quantification and target detection in tissue and drug delivery, the applications of combined FLIM and EPR measurements are versatile and future applications are numerous. The DL platform can be applied to any system, where spatial resolution combined with knowledge about concentration and local environment is required. For instance, the deactivation of the EPR label could act as a sensor for the production of reactive oxygen species,[29] while the FLIM label allows the simultaneous localization of the DL within the cellular environment.[30] Also, photodynamic therapy in conjunction with the use of photosensitizers are feasible.[31] Similarly, we envision the use of the DL compound in in vitro experiments to provide new and unprecedented insight into biomolecular dynamics, structure, and interactions. Thus, we hope that this multi read-out labeling platform paves the way for future studies in which the complementary information from FLIM and EPR enables comprehensive characterization of any target system.

Acknowledgements

This work was financially supported by the German Research Foundation (Collaborative Research Center 1112, Project B01 to P.D., S.B.L., and M.C.M., B03 to U.A., C02 to M.S.K, and A04 to M.C., and partially by Collaborative Research Center 1078, Project A2, and Collaborative Research Center 1449 to U.A.). We would like to acknowledge the assistance of the Core Facility BioSupraMol supported by the DFG and thank Dr. A. Springer. M.C. acknowledges IKERBASQUE-Basque Foundation for Science and MINECO project RTI2018-099227-B-I00 for financial support. E.R.O.-B. gratefully thanks the Dahlem Research School for a scholarship. P.D. thanks the China Scholarship Council for financial support. Open access funding enabled and organized by Projekt DEAL.

Conflict of interest

The authors declare no conflict of interest.

Keywords: 3-carboxy-proxyl (PCA) · fluorescence · multiplexed FLIM–EPR spectroscopy · Rhodamine B · spin labels

[1] M. Schäfer-Korting, C. Zoschke, *Handbook of Experimental Pharmacology*, Springer, Berlin, **2020**, pp. 1–28.
[2] P. Dong, F. F. Sahle, S. B. Lohan, S. Saeidpour, S. Albrecht, C. Teutloff, R. Bodmeier, M. Unbehauen, C. Wolff, R. Haag, J. Lademann, A. Patzelt, M. Schäfer-Korting, M. C. Meinke, *J. Controlled Release* **2019**, *295*, 214–222.
[3] P. Kuppusamy, P. Wang, M. Chzhan, J. L. Zweier, *Magn. Reson. Med.* **1997**, *37*, 479–483.
[4] Y. Tang, X. Kong, A. Xu, B. Dong, W. Lin, *Angew. Chem. Int. Ed.* **2016**, *55*, 3356–3359; *Angew. Chem.* **2016**, *128*, 3417–3420.
[5] a) S. Kaščáková, S. de Visscher, B. Kruijt, H. S. de Bruijn, A. van der Ploeg-van den Heuvel, H. J. Sterenborg, M. J. Witjes, A. Amelink, D. J. Robinson, *Lasers Med. Sci.* **2011**, *26*, 789–801; b) K. R. Diamond, P. P. Malysz, J. E. Hayward, M. S. Patterson, *J. Biomed. Opt.* **2005**, *10*, 0240070; c) M. Gurfinkel, A. B. Thompson, W. Ralston, T. L. Troy, A. L. Moore, T. A. Moore, J. D. Gust, D. Tatman, J. S. Reynolds, B. Muggenburg, K. Nikula, R. Pandey, R. H. Mayer, D. J. Hawrysz, E. M. Sevick-Muraca, *Photochem. Photobiol.* **2000**, *72*, 94–102; d) P. Volz, P. Schilrreff, R. Brodwolf, C. Wolff, J. Stellmacher, J. Balke, M. J. Morilla, C. Zoschke, M. Schäfer-Korting, U. Alexiev, *Ann. N. Y. Acad. Sci.* **2017**, *1405*, 202–214.
[6] a) J. W. Borst, A. J. W. G. Visser, *Meas. Sci. Technol.* **2010**, *21*, 102002–102024; b) M. Y. Berezin, S. Achilefu, *Chem. Rev.* **2010**, *110*, 2641–2684; c) U. Alexiev, P. Volz, A. Boreham, R. Brodwolf, *Eur. J. Pharm. Biopharm.* **2017**, *116*, 111–124; d) L. M. Hirvonen, J. Nedbal, N. Almutairi, T. A. Phillips, W. Becker, T. Conneely, J. Milnes, S. Cox, S. Sturzenbaum, K. Suhling, *J. Biophotonics* **2019**, *13*, e201960099.
[7] B. W. Herman, X. F. Wodnicki, P. Perisamy, A. Mahajan, N. Berry, G. Gordon in *Applied Fluorescence in Chemistry, Biology and Medicine*, *Vol. 1* (Ed.: W. Rettig, B. Strehmel, S. Schrader, H. Seifert), Springer-Verlag Berlin Heidelberg, Heidelberg, **1999**, p. 562.
[8] R. Brodwolf, P. Volz-Rakebrand, J. Stellmacher, C. Wolff, M. Unbehauen, R. Haag, M. Schäfer-Korting, C. Zoschke, U. Alexiev, *Theranostics* **2020**, *10*, 6322–6336.

[9] a) A. Boreham, J. Pikkemaat, P. Volz, R. Brodwolf, C. Kuehne, K. Licha, R. Haag, J. Dernedde, U. Alexiev, *Molecules* **2015**, *21*, E22; b) C. Richter, C. Schneider, M. T. Quick, P. Volz, R. Mahrwald, J. Hughes, B. Dick, U. Alexiev, N. P. Ernsting, *Phys. Chem. Chem. Phys.* **2015**, *17*, 30590 – 30597; c) J. Balke, P. Volz, F. Neumann, R. Brodwolf, A. Wolf, H. Pischon, M. Radbruch, L. Mundhenk, A. D. Gruber, N. Ma, U. Alexiev, *Small* **2018**, *14*, 1800310; d) K. Kirchberg, T. Y. Kim, M. Moller, D. Skegro, G. Dasara Raju, J. Granzin, G. Büldt, R. Schlesinger, U. Alexiev, *Proc. Natl. Acad. Sci. USA* **2011**, *108*, 18690 – 18695; e) K. Ober, P. Volz-Rakebrand, J. Stellmacher, R. Brodwolf, K. Licha, R. Haag, U. Alexiev, *Langmuir* **2019**, *35*, 11422 – 11434; f) L. Gronbach, C. Wolff, K. Klinghammer, J. Stellmacher, P. Jurmeister, U. Alexiev, M. Schäfer-Korting, I. Tinhofer, U. Keilholz, C. Zoschke, *Biomaterials* **2020**, *258*, 120277.

[10] a) S. Saeidpour, S. B. Lohan, M. Anske, M. Unbehauen, E. Fleige, R. Haag, M. C. Meinke, R. Bittl, C. Teutloff, *Eur. J. Pharm. Biopharm.* **2017**, *116*, 94 – 101; b) S. Saeidpour, S. B. Lohan, A. Solik, V. Paul, R. Bodmeier, G. Zoubari, M. Unbehauen, R. Haag, R. Bittl, M. C. Meinke, C. Teutloff, *Eur. J. Pharm. Biopharm.* **2017**, *110*, 19 – 23.

[11] a) B. Joseph, A. Sikora, E. Bordignon, G. Jeschke, D. S. Cafiso, T. F. Prisner, *Angew. Chem. Int. Ed.* **2015**, *54*, 6196 – 6199; *Angew. Chem.* **2015**, *127*, 6294 – 6297; b) F. Bertoli, G. L. Davies, M. P. Monopoli, M. Moloney, Y. K. Gun'ko, A. Salvati, K. A. Dawson, *Small* **2014**, *10*, 3307 – 3315; c) W. L. Hubbell, D. S. Cafiso, C. Altenbach, *Nat. Struct. Biol.* **2000**, *7*, 735 – 739; d) S. C. Kohout, S. Corbalan-Garcia, J. C. Gomez-Fernandez, J. J. Falke, *Biochemistry* **2003**, *42*, 1254 – 1265; e) C. Braem, T. Blaschke, G. Panek-Minkin, W. Herrmann, P. Schlupp, T. Paepenmuller, C. Muller-Goyman, W. Mehnert, R. Bittl, M. Schäfer-Korting, K. D. Kramer, *J. Controlled Release* **2007**, *119*, 128 – 135.

[12] S. Kilic, S. Felekyan, O. Doroshenko, I. Boichenko, M. Dimura, H. Vardanyan, L. C. Bryan, G. Arya, C. A. M. Seidel, B. Fierz, *Nat. Commun.* **2018**, *9*, 235.

[13] a) N. Alnasif, C. Zoschke, E. Fleige, R. Brodwolf, A. Boreham, E. Rühl, K. M. Eckl, H. F. Merk, H. C. Hennies, U. Alexiev, R. Haag, S. Küchler, M. Schäfer-Korting, *J. Controlled Release* **2014**, *185*, 45 – 50; b) A. Vogt, C. Wischke, A. T. Neffe, N. Ma, U. Alexiev, A. Lendlein, *J. Controlled Release* **2016**, *242*, 3 – 15; c) J. Frombach, M. Unbehauen, I. N. Kurniasih, F. Schumacher, P. Volz, S. Hadam, F. Rancan, U. Blume-Peytavi, B. Kleuser, R. Haag, U. Alexiev, A. Vogt, *J. Controlled Release* **2019**, *299*, 138 – 148.

[14] S. B. Lohan, N. Icken, C. Teutloff, S. Saeidpour, R. Bittl, J. Lademann, E. Fleige, R. Haag, S. F. Haag, M. C. Meinke, *Int. J. Pharm.* **2016**, *501*, 271 – 277.

[15] E. Beetge, J. du Plessis, D. G. Muller, C. Goosen, F. J. van Rensburg, *Int. J. Pharm.* **2000**, *193*, 261 – 264.

[16] a) E. London, *Mol. Cell. Biochem.* **1982**, *45*, 181 – 188; b) A. Chattopadhyay, E. London, *Biochemistry* **1987**, *26*, 39 – 45; c) N. V. Blough, D. J. Simpson, *J. Am. Chem. Soc.* **1988**, *110*, 1915 – 1917; d) N. Barhate, P. Cekan, A. P. Massey, S. T. Sigurdsson, *Angew. Chem. Int. Ed.* **2007**, *46*, 2655 – 2658; *Angew. Chem.* **2007**, *119*, 2709 – 2712.

[17] a) K. Yamamoto, A. Klossek, R. Flesch, T. Ohigashi, E. Fleige, F. Rancan, J. Frombach, A. Vogt, U. Blume-Peytavi, P. Schrade, S. Bachmann, R. Haag, S. Hedtrich, M. Schäfer-Korting, N. Kosugi, E. Rühl, *J. Controlled Release* **2016**, *242*, 64 – 70; b) F. Rancan, Q. Gao, C. Graf, S. Troppens, S. Hadam, S. Hackbarth, C. Kembuan, U. Blume-Peytavi, E. Ruhl, J. Lademann, A. Vogt, *ACS Nano* **2012**, *6*, 6829 – 6842; c) M. O. Danso, T. Berkers, A. Mieremet, F. Hausil, J. A. Bouwstra, *Exp. Dermatol.* **2015**, *24*, 48 – 54; d) V. Planz, C.-M. Lehr, M. Windbergs, *J. Controlled Release* **2016**, *242*, 89 – 104.

[18] C. Zoschke, M. Ulrich, M. Sochorová, C. Wolff, K. Vávrová, N. Ma, C. Ulrich, J. M. Brandner, M. Schäfer-Korting, *J. Controlled Release* **2016**, *233*, 10 – 18.

[19] C. H. Wong, K. W. Siah, A. W. Lo, *Biostatistics* **2019**, *20*, 273 – 286.

[20] H. R. Krüger, G. Nagel, S. Wedepohl, M. Calderón, *Nanoscale* **2015**, *7*, 3838 – 3844.

[21] N. O. Mchedlov-Petrossyan, T. A. Cheipesh, A. D. Roshal, A. O. Doroshenko, N. A. Vodolazkaya, *Methods Appl. Fluoresc.* **2016**, *4*, 034002.

[22] R. Mercadé-Prieto, L. Rodriguez-Rivera, X. D. Chen, *Photochem. Photobiol. Sci.* **2017**, *16*, 1727 – 1734.

[23] a) T. López Arbeloa, F. López Arbeloa, P. Hernández Bartolome, I. López Arbeloa, *Chem. Phys.* **1992**, *160*, 123 – 130; b) D. Magde, G. E. Rojas, P. G. Seybold, *Photochem. Photobiol.* **1999**, *70*, 737 – 744.

[24] A. S. Kristoffersen, S. R. Erga, B. Hamre, Ø. Frette, *J. Fluoresc.* **2014**, *24*, 1015 – 1024.

[25] J. Möser, K. Lips, M. Tseytlin, G. R. Eaton, S. S. Eaton, A. Schnegg, *J. Magn. Reson.* **2017**, *281*, 17 – 25.

[26] N. Otberg, H. Richter, H. Schaefer, U. Blume-Peytavi, W. Sterry, J. Lademann, *J. Invest. Dermatol.* **2004**, *122*, 14 – 19.

[27] J. Lehner, S. Stoll, *J. Chem. Phys.* **2020**, *152*, 094103.

[28] R. Schulz, K. Yamamoto, A. Klossek, R. Flesch, S. Honzke, F. Rancan, A. Vogt, U. Blume-Peytavi, S. Hedtrich, M. Schäfer-Korting, E. Rühl, R. R. Netz, *Proc. Natl. Acad. Sci. USA* **2017**, *114*, 3631 – 3636.

[29] A. Elpelt, S. Albrecht, C. Teutloff, M. Hüging, S. Saeidpour, S. B. Lohan, S. Hedtrich, M. C. Meinke, *Chem.-Biol. Interact.* **2019**, *310*, 108752.

[30] A. V. Kuznetsov, I. Kehrer, A. V. Kozlov, M. Haller, H. Redl, M. Hermann, M. Grimm, J. Troppmair, *Anal. Bioanal. Chem.* **2011**, *400*, 2383 – 2390.

[31] P. H. Guelluy, M. P. Fontaine-Aupart, A. Grammenos, S. Lecart, J. Piette, M. Hoebeke, *Photochem. Photobiol. Sci.* **2010**, *9*, 1252 – 1260.

Manuscript received: September 22, 2020
Revised manuscript received: November 27, 2021
Accepted manuscript online: February 5, 2021
Version of record online: May 26, 2021

